

Non-precursory Accelerating Aseismic Slip during Rupture Nucleation

Xiaoyu Wang¹, Luca Dal Zilio¹, Julia Morgan², and David S. Kammer¹

¹ETH Zurich

²Department of Earth Science, Rice University, Houston, Texas, USA

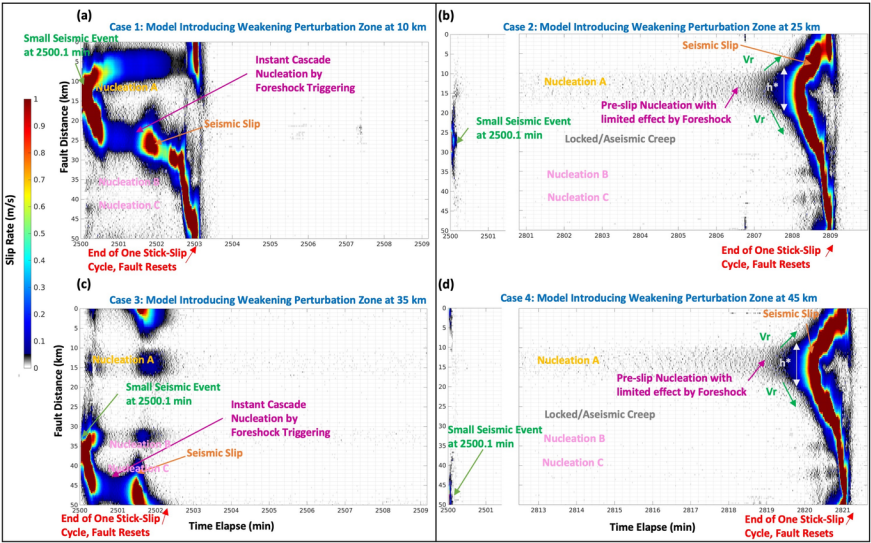
December 7, 2022

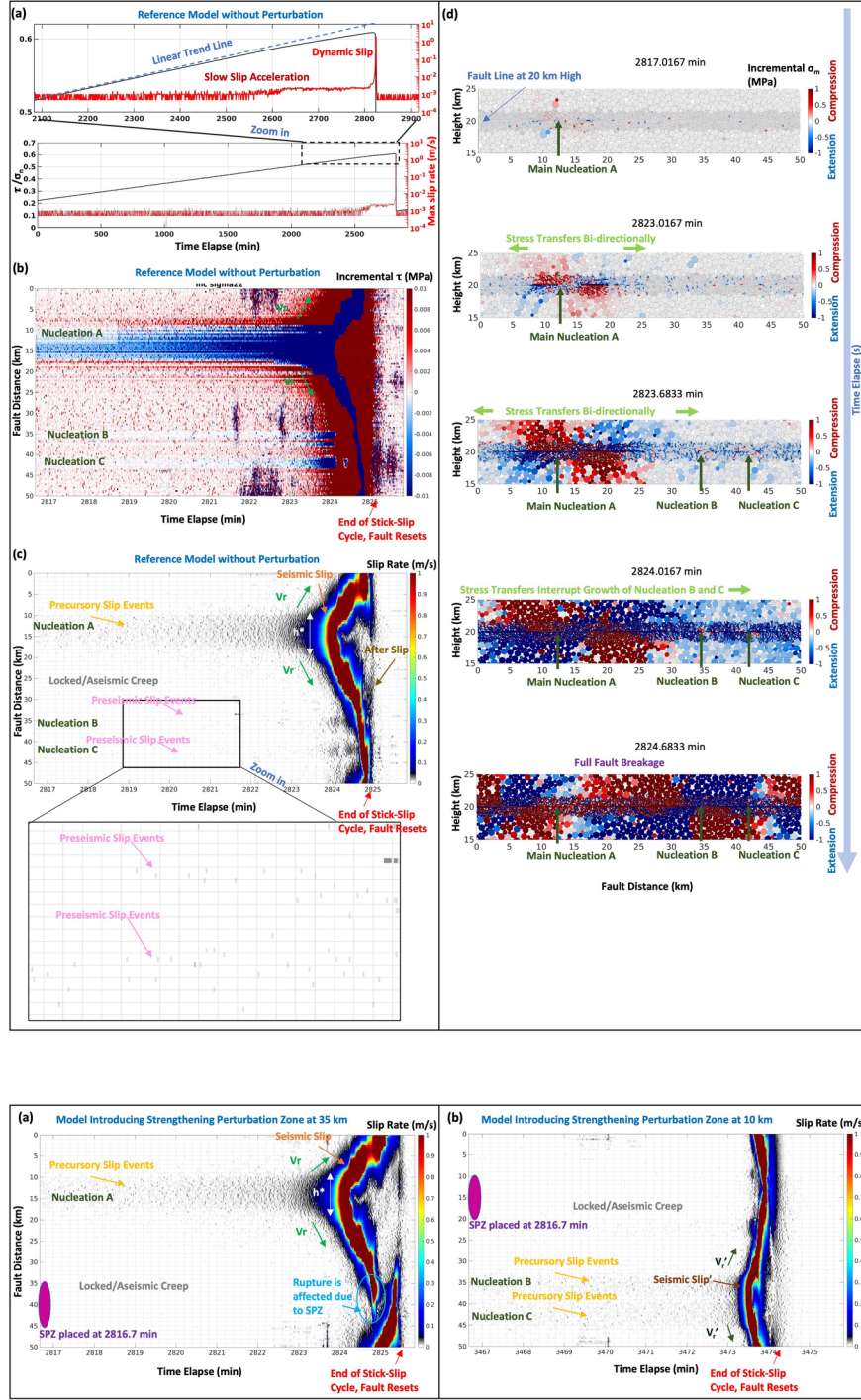
Abstract

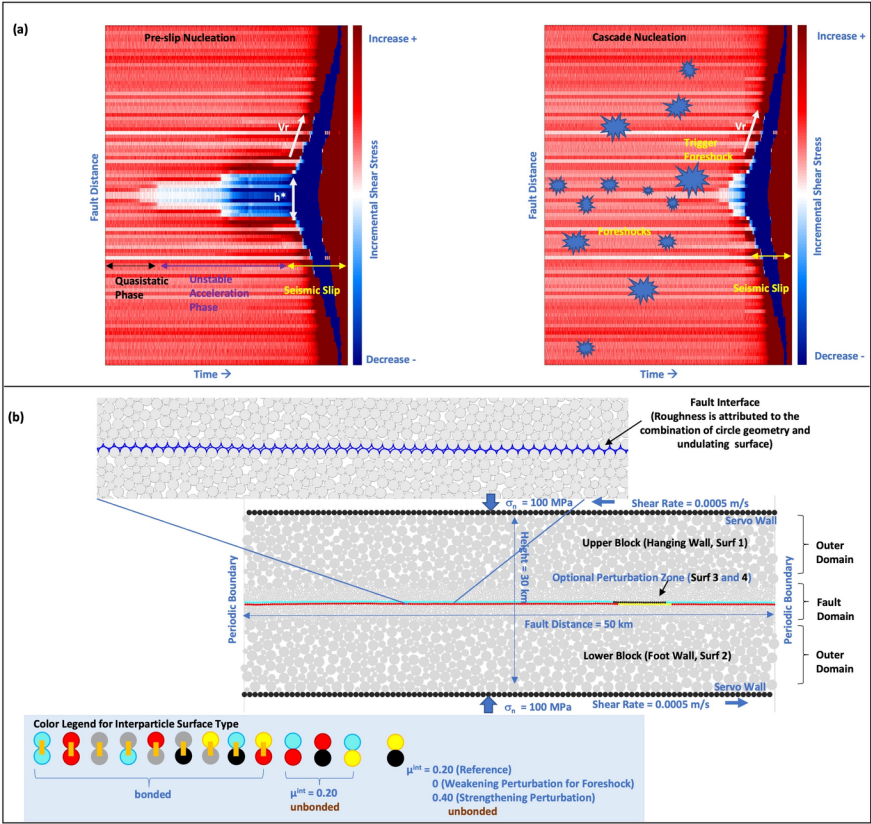
Accelerating aseismic slip events have been commonly observed during the rupture nucleation processes of the earthquake. While that accelerating aseismic slip is usually considered strong evidence for precursory activity, it remains unclear whether all accelerating aseismic slip events are precursory to an incoming earthquake. Two contrasting nucleation models have been introduced to explain the observations associated with the nucleation of unstable slip: the pre-slip and cascade nucleation models. Each of these two-end members, however, has its own limitations. In this study, we employ Discrete Element Method (DEM) simulations of a 2-D strike-slip fault to simulate various rupture nucleation and triggering processes. Our simulation results manifest that the final seismic event is a product contributed by multiple pre-slip nucleation sites, which may interact, causing clock advance or cascade nucleation rupture processes. We also introduce a strengthening perturbation zone to investigate the role of a single nucleation site in an imminent seismic event. The simulation results reveal a new type of non-precursory aseismic slip, representing the region favoring the generation of the precursory slip process but not correlating to the incoming main event, which differs from the previous interpretation of precursory slip. Furthermore, we include weakening perturbation zones in some simulations to demonstrate how small earthquakes may or may not trigger a nucleation site depending on spatial and temporal conditions. Our simulation results imply that such non-precursory but accelerating aseismic slip events may suggest a fault segment that appears weakly coupled but possesses the potential to be triggered seismically.

Hosted file

essoar.10512893.1.docx available at <https://authorea.com/users/564116/articles/611092-non-precursory-accelerating-aseismic-slip-during-rupture-nucleation>







Non-precursory Accelerating Aseismic Slip during Rupture Nucleation

Xiaoyu Wang¹, Luca Dal Zilio², Julia K. Morgan³, David S. Kammer¹

¹ Institute for Building Materials, ETH Zurich, Switzerland

² Institute of Geophysics, ETH Zurich, Switzerland

³ Department of Earth, Environmental and Planetary Sciences, Rice University, US

Corresponding author: David S. Kammer (dkammer@ethz.ch)

Key Points:

- Aseismic and seismic slip events and their interactions are simulated in particle-based models.
- Regions favoring a generation of precursory accelerating slip can have a minimal effect on the incoming main seismic event.
- Accelerating non-precursory aseismic slip may indicate a large seismic potential that a preceding seismic event can trigger.

Keywords

Precursory slip processes, Rupture nucleation, Seismic and aseismic Slip, Discrete element models, Shearing test

Abstract

Accelerating aseismic slip events have been commonly observed during the rupture nucleation processes of the earthquake. While that accelerating aseismic slip is usually considered strong evidence for precursory activity, it remains unclear whether all accelerating aseismic slip events are precursory to an incoming earthquake. Two contrasting nucleation models have been introduced to explain the observations associated with the nucleation of unstable slip: the pre-slip and cascade nucleation models. Each of these two-end members, however, has its own limitations. In this study, we employ Discrete Element Method (DEM) simulations of a 2-D strike-slip fault to simulate various rupture nucleation and triggering processes. Our simulation results manifest that the final seismic event is a product contributed by multiple pre-slip nucleation sites, which may interact, causing clock advance or cascade nucleation rupture processes. We also introduce a strengthening perturbation zone to investigate the role of a single nucleation site in an imminent seismic event. The simulation results reveal a new type of non-precursory aseismic slip, representing the region favoring the generation of the precursory slip process but not correlating to the incoming main event, which differs from the previous interpretation of precursory slip. Furthermore, we include weakening perturbation zones in some simulations to demonstrate how small earthquakes may or may not trigger a nucleation site depending on spatial and temporal conditions. Our simulation results imply

that such non-precursory but accelerating aseismic slip events may suggest a fault segment that appears weakly coupled but possesses the potential to be triggered seismically.

1 Introduction

An important contribution to improving our local seismic hazard assessment is our understanding of rupture nucleation in active fault regions (Dieterich, 1992). These nucleation processes are complex and essentially related to many important open questions in earthquake science, including how an earthquake initiates and how to predict an incoming one (Kato & Ben-Zion, 2021; McLaskey, 2019). For example, active faults display a rich slip spectrum during earthquake nucleation, as well as between two main seismic events (Leeman et al., 2016; Peng & Gombert, 2010), including widespread creep, localized aseismic slip events, and intensifying microseismicity prior to the mainshock (Dragert et al., 2001; Hawthorne & Bartlow, 2018; Ozawa et al., 2002). A seismic rupture also may start progressively with a slow unlocking of a heterogeneous fault interface, causing foreshocks and precursory aseismic slip (Cattania & Segall, 2021; Noda et al., 2013; Yabe & Ide, 2018). Furthermore, accelerating aseismic slip clusters during intensifying foreshock sequences have been observed before many moderate and large earthquakes (Cattania & Segall, 2021; Kato et al., 2012; Trugman & Ross, 2019). All of those observations suggest that a range of processes are involved in earthquake rupture nucleation. However, we still lack a clear understanding of the physical mechanisms driving these precursory phases during the rupture nucleation.

One prominent model, the pre-slip nucleation model, was proposed to explain the onset of a dynamic rupture, based on lab observations (McLaskey & Lockner, 2014; Ohnaka & Kuwahara, 1990; Yamashita et al., 2021) and theoretical modeling (Ampuero & Rubin, 2008; Dieterich, 1978; Lapusta & Rice, 2003). In this model, the nucleation begins from a quasi-static phase, where a reduced shear stress (τ) region represents growing aseismic slip clusters (Figure 1a). The spatial expansion of the preseismic slip clusters accelerates and approaches a critical nucleation length (h^*), eventually leading to seismic rupture over the active fault (Figure 1a). Conceptually, there is a temporal and spatial transition from aseismic slip transients to large seismic events, making it plausible to assess the incoming seismic events. The hastened aseismic slip phase prior to large earthquakes has been revealed by geodetic and seismic monitoring of active tectonic fault systems (Ruiz et al., 2014; Socquet et al., 2017; Tape et al., 2018). Nevertheless, most reported seismic events in nature displayed no apparent transitions between aseismic slip and seismic slip (Guérin-Marthe et al., 2019; McLaskey, 2019). Therefore, the pre-slip model may be oversimplified and inappropriate for characterizing all rupture nucleation processes along heterogeneous interfaces.

Alternatively, a cascade nucleation model was introduced to characterize a stochastic correlation of a small nucleation phase to an unexpectedly large dynamic slip (Ellsworth & Beroza, 1995; Olson & Allen, 2005). This model sug-

gests that small earthquakes (foreshocks) initiating at small brittle patches kick the surrounding strong asperities randomly (Figure 1a). Eventually, one or a few of them trigger a large seismic event, which makes assessing an upcoming main shock particularly challenging (Noda et al., 2013). However, the cascade model fails to characterize the preseismic slow slip transients as observed in some laboratory experiments and theoretical studies of fault slip on a frictional surface (Dieterich, 1992; McLaskey, 2019). Moreover, it fails to explain well the interactions among multiple nucleation sites and the interplay between slow-slip transients and seismic slip. In fact, a rupture initiation may present behavior that lies between the pre-slip and cascade models (Cattania & Segall, 2021). Therefore, a model that reconciles the two nucleation models to describe better the rupture process is needed.

Interestingly, the pre-slip nucleation model implies that the presence of precursory aseismic slip is directly responsible for the incoming dynamic rupture. Such a hypothesis is evident from a few observations of aseismic slip sequences and their corresponding foreshock intensifications before large earthquakes (Dalaison et al., 2021; Kato et al., 2012; Socquet et al., 2017). In contrast to the precursory slip processes, many preseismic slip processes are non-precursory, having a limited effect on the upcoming seismic event. A typical non-precursory aseismic slip event experiences both slip rate acceleration and deceleration, yet it never turns into a large earthquake (Barker et al., 2018; Caniven et al., 2021). Besides the typical non-precursory aseismic slip, some preseismic slip sequences may behave as precursory slip events while having a limited effect on the incoming seismic ruptures. For example, multiple clusters of accelerating aseismic slip sequences have been observed before the main events along natural faults (Dalaison et al., 2021; Hasegawa & Yoshida, 2015; Socquet et al., 2017), as well as in numerical simulations (Albertini et al., 2021; Caniven et al., 2021; Cattania & Segall, 2021). However, it remains unclear whether all of those accelerating aseismic slip events are directly related to the incoming main shock and also how each may influence the following seismicity. Therefore, careful studies on precursory slip processes are still needed to improve our ability to assess incoming seismic events.

To better characterize the rupture preparation processes and investigate their corresponding aseismic slip, this study employs Discrete Element Method (DEM) simulations of a strike-slip fault in a two-dimensional (2D) domain to simulate rupture nucleation. Our models simulate aseismic (slow) and dynamic (fast) slip, on dilatant particle-based fault interfaces. This study aims to 1) propose a rupture nucleation process that reconciles both pre-slip and cascade nucleation models, 2) demonstrate the interactions and triggering among nucleation sites by tracking the stress evolution and displacement through the rupture preparation process, 3) differentiate precursory aseismic (slow) slip from accelerating aseismic slip sequences, and 4) investigate the types of preseismic slow slip sequences, their relations to the two-end member nucleation modes, and their implication for incoming seismic events.

2 Approach and Methodology

2.1 Numerical Method

To complement the limited geophysical observations and to link laboratory experiments to natural systems, state-of-the-art numerical simulations of fault slip have simulated cycles of dynamic and aseismic slip resulting from tectonic loading. For instance, continuum-based models have explicitly implemented a rate and state friction law (RSF), yet typically allow for limited fault motion along a single, infinite, and thin planar fault embedded in an elastic half-space (Barbot, 2019; Cattania & Segall, 2021; Lapusta & Rice, 2003; Rice et al., 2001). Alternatively, discontinuum approaches have been developed to simulate a range of slip modes (Ferdowsi & Rubin, 2020; Romanet et al., 2018; Van den Ende et al., 2018) while also accounting for effects of the fault roughness on the slip behavior. The Discrete Element Method (DEM) is one of these methods and has been used to explore how the topographic roughness and corresponding dilatant deformation influence the aseismic and dynamic slip (Blank et al., 2021; Caniven et al., 2021).

Here, we use DEM, a particle-based discontinuous numerical modeling approach to simulate unlimited fault motions, including aseismic (slow) and dynamic (fast) slip on a rough fault interface. We use RICEBAL, which is the program initially developed and described by (Morgan, 2015). In a DEM assemblage, discrete particles are modeled as compressible elastic spheres interacting with each other, governed by the Hertz-Mindlin contact theory (Johnson, 1987; Morgan, 2015). Once the particles come into contact, shear (f_s) and normal (f_n) forces on the interparticle contacts are calculated. The f_s is limited by the predefined interparticle friction coefficient (μ_{part}). At each time step, the normalized components of all contact forces acting on each particle are summed to derive the net force. The model then solves the linear vector equation of Newton’s second law of motion for each particle, along with its angular counterpart, updating the new position and orientation of the particle over each time step.

Additionally, cohesion can be introduced by adding numerical bonds to simulate unbreakable elastic domains (Caniven et al., 2021; Morgan, 2015). Each numerical bond connects the centers of two particles in contact, acting as two elastic springs and an elastic beam that transmit normal and shear forces and moment. The corresponding equations are provided in the supplementary materials (S1). A full description of DEM methodology can also be found in Morgan (2015).

2.2 Model Setups

This study deploys DEM to simulate a rough fault interface with strong asperities. We construct a 50-kilometer vertical strike-slip fault to simulate complete rupture nucleation processes and their interactions in a tectonic system (Figure 1b). Every model system consists of two domains: a fault domain and the outer domain. The outer domain comprises relatively coarse particles with radii of 250, 350, and 500 m, and the near-fault region is made of particles with radii of 75 m and 100 m (Figure 1b). The top and bottom boundaries are servo walls

that apply constant compressive normal stress and shearing rate to the model. The lateral boundaries are periodic to minimize any boundary effects. The complete simulation workflow is conducted through consolidation and shearing test phases, which are explained below.

In the consolidation phase, a fault interface is first defined by two rows of uniform size particles with a radius of 100 m, creating a series of geometric asperities to yield fault slips (Caniven et al., 2021; Sainoki & Mitri, 2016). The particles defined in the two rows are initially fixed to inhibit any motion or rotation to maintain a relatively straight line for each row, simulating a simplified high-dilatancy rough interface. The meter-scale geometric asperities in the kilometer-scale model are analogues for geologic morphology, such as seafloor roughness in subduction zones (Bilek et al., 2003). The interparticle friction coefficient (μ_{part}) for the domain is 0.7 during the consolidation phase (Vora & Morgan, 2019). A constant normal stress of 100 MPa is applied to the top and bottom servo walls to simulate the overburden pressure as the volume consolidates. The particles are tightly packed by the end of the consolidation. Once there is no further motion and rotation, strong numerical bonds are added to the upper (hanging wall) and lower (footwall) blocks, whereas there is no bond along the fault interface (Figure 1b). Therefore, no plastic deformation will develop elsewhere within the lower or upper blocks. Generally, each block behaves as an elastic medium, transmitting far-field stresses from the servo walls to the fault domain.

After adding the strong bonds, the lines of particles that define the fault interface are unfixed and run through multiple simulation cycles before the shearing test phase to ensure the system is subjected to a stabilized normal stress of 100 MPa. Concurrently, the interparticle friction coefficient (μ_{part}) along the fault interface is set to 0.2, which combined with particle-particle interlocking yields a maximum bulk friction coefficient of ~ 0.6 for the sliding interface (Figure 2a), comparable to the frictional strength for regular fault zones (Byerlee, 1978). The mechanical properties of the particles are based on previous DEM modeling for granite (Vora & Morgan, 2019), and the mechanical properties of the numerical bonds are based on the published numerical shearing experiments (Caniven et al., 2021). Details about those key modeling parameters can be found in the supplementary materials (Table S1). A constant velocity of 0.5 mm/s is imposed at the servo walls, producing intermittent locking and unlocking along the fault. Such shearing rate is able to generate geologically reasonable values for slow and fast slip events on the sliding interface (Ferdowsi & Rubin, 2020).

To maintain DEM system stability, the simulation's time step (TS) must be a fraction of the lowest collision time of the particle (Shäfer et al., 1996). The collision time for the particle governed by the Hertzian contact law in an elastic medium can be derived by using the equation below:

$$t_n = 3.21 \left(\frac{3m_{eff}}{4\sqrt{R_{eff}E_{eff}}} \right)^{2/5} v_n^{-1/5} \quad (1)$$

Here, v_n is the impact particle velocity, $m_{eff} = (m_1 m_2) / (m_1 + m_2)$, $R_{eff} =$

$(R_1 R_2)/(R_1 + R_2)$, and $E_{\text{eff}} = 1/[(1 - v_1^2)/E_1 + (1 - v_2^2)/E_2]$, where m_1 and m_2 are masses, R_1 and R_2 are radii, E_1 and E_2 are the Young's Moduli, and v_1 and v_2 are Poisson's ratios of two particles in contact. Therefore, a stable time step of 0.01 seconds per iteration cycle is determined based on the estimation that the maximum impact particle velocity (v_n) is ~ 10 m/s in the system.

2.3 Perturbation Zone

In addition to our reference simulations, we perform numerical experiments in which we impose either a weaker or stronger fault patch (particles in black and yellow in the fault zone in Figure 1b) to trigger a small earthquake or minimize the effect of specific nucleation sites on subsequent seismic events.

A weakening perturbation zone (WPZ) can be introduced to induce the onset of a small seismic event at a specific temporal and spatial point. The approach has been employed to simulate dynamic weakening in the previous work (Wang et al., 2021), where the value of μ_{part} assigned to the contacts within a certain fault length is decreased directly. The instantaneous reduction in friction along the fault simulates a change from static to dynamic friction during an earthquake (Rabinowicz, 1951). Similarly, we can introduce a strengthening perturbation zone (SPZ) by increasing μ_{part} within a certain fault domain to impede the growth of the unwanted nucleation sites and their corresponding preseismic slow slip. Using this approach, we are able to focus on a particular nucleation process, examining the causal relationship between one cluster of aseismic slip events and the incoming seismic event.

3 Simulation Results

The position and force components of each particle are documented over simulation time. The corresponding stress components, then, are resolved to calculate the displacement rate, the mean (σ_m), shear (τ), and normal (σ_n) stresses of each particle in the fault zone. Details about their calculations can be found in prior work (Morgan, 2015; Wang et al., 2021). Following previous work (McLaskey, 2019), we define the particle displacement rate to be dynamic when the corresponding rupture front velocity (V_r) is over 10% of the shear wave velocity. This corresponds to approximately 0.1 m/s in our numerical simulations as $V_r = \sim 300$ m/s. Hence, the rate of aseismic (slow) slip is given by < 0.1 m/s in our simulation results. The rupture front velocity (V_r), which indicates the growth rate of the area with reduced τ , can be derived from the time-space map of incremental τ (pre-slip nucleation model in Figure 1a) based on the equation:

$$V_r = 1/|\partial t_r(x)/\partial x| \quad (2)$$

Here, t_r is the temporal increment (time), and x is the distance along the fault.

3.1 Reference Model with Constant Pre-assigned μ_{part} along Fault Plane

We first build a 50-km vertical strike-slip fault without any perturbation as a reference model. The evolution of the ratio of normal to shear stress (τ/σ_n) and maximum slip rate are plotted respectively in Figure 2a. As the two lines of

particles alternate between an interlocking to a loose state during the asperity shearing, the model yields multiple regular stick-slip behaviors, including main seismic events and interseismic periods. We define the elapsed time as the time since the last main seismic event (Figure 2a). As the fault approaches the instability (from ~ 2100 min, in Figure 2a), the curve of τ/τ_n starts to depart from a linear trend, indicating a slow stress drop (Figure 2a). Concurrently, the slip rate accelerates gradually, and a jump in maximum slip rate occurs at ~ 2600 min, which is shortly before a macroscopic failure occurs (red curves in Figure 2a). Previous numerical studies and laboratory experiments also observed a similar departure of τ/τ_n from linearity (Caniven et al., 2021; McLaskey & Lockner, 2014), indicating the occurrence of precursory aseismic slip.

The time-space maps of incremental τ and slip rate along the fault plane are plotted in Figures 2b and 2c, respectively. Moreover, we plot the incremental changes in τ_n near the fault to demonstrate stress transfer, as well as localized compressional and extensional states through the rupture nucleation process. (Figure 2d). An apparent strike-slip focal mechanism initiates at ~ 12 km (Figure 2d), indicating a distinct nucleation event (Nucleation A). Simultaneously, two additional small nucleation events (Nucleation B and C) initiate at about 35 km and 42 km, respectively (Figures 2b and 2d). Nucleation A first approaches a critical state (at ~ 2823 min), where the rupture front propagation rate reaches (V_r) over 300 m/s (Figure 2b). It grows rapidly and propagates laterally through the acceleration of the preseismic slow slip sequences. (Figures 2c and 2d). Moreover, the blue regions associated with Nucleation B and C turn red during dynamic rupture in Figure 2c. It is likely that the rupture first initiates with Nucleation A, interrupting the growth of Nucleation B and Nucleation C. During the seismic event (after 2824 min), the V_r is over 1 km/s, and the maximum slip rate is over 1 m/s (Figure 2c). Eventually, the seismic rupture broke the entire fault zone and restored the system.

Interestingly, previous numerical studies also observed similar phenomena, where multiple nucleation sites grow concurrently prior to a final dynamic rupture (Albertini et al., 2021; Caniven et al., 2021; Cattania & Segall, 2021). However, the preseismic slow slip clusters and the subsequent seismicities in the nucleation regions were not defined well. All preseismic slip processes were often interpreted as precursory slip events for the upcoming seismic event. In our model, however, Nucleation A appears to have reached its critical nucleation state ($V_r > 300$ m/s) much earlier than Nucleation B and C (Figures 2b and 2c).

3.2 Differentiating Precursory Slow Slip Sequences

To determine whether all the preseismic slow slip events are directly correlated to the incoming dynamic slip event, we define a strengthening perturbation zone (SPZ), where μ^{part} is increased from 0.20 to 0.40 ~ 350 sec before the seismic event (at 2816.7 min in Figure 3), impeding the development of nucleation if there is any. Concurrently, the frictional strength is maintained elsewhere along the fault interface.

First, we place a 10-km wide SPZ at 35 km to test whether the preseismic slow slip events in Nucleation B and Nucleation C play a key role in generating the incoming dynamic slip. As shown in Figure 3a, their nucleation growth diminishes while dynamic slip still occurs at about the same time (Figure 3a), consistent with the reference model (Figure 2c). Moreover, the slip pattern and its amplitude remain almost unchanged, indicating that the dynamic slip event without the contribution of Nucleation B and C (Figure 3a) is identical to the one observed in the reference model (Figure 2c). In general, the dynamic slip initiates from Nucleation A and is essentially controlled by it. Therefore, Nucleation B and Nucleation C have a limited effect on the nucleation of the upcoming dynamic slip event, implying that the preseismic slow slip events within Nucleation B and Nucleation C are not precursory for the incoming seismic event.

In another case, we place the 10-km wide SPZ at 10 km to minimize the influence of Nucleation A to better define the preseismic slow slip sequences in Nucleation B and C (Figure 3b). Nucleation B and C continue their evolution as the early interruption originating from Nucleation A no longer exists. The aseismic slip events in Nucleation B and C eventually turn into a large dynamic rupture, propagating across the entire stretch of the fault seismically at ~ 3473.2 min, approximately 650 minutes later than the reference rupture (Figure 3b). The seismic slip pattern differs from the reference model, indicating further that the aseismic slip events in Nucleation B and Nucleation C lead up to a new seismic event, governed by pre-slip nucleation mode (Figure 3b). In the reference model (Figure 2b), Nucleation B and Nucleation C are triggered by the seismic rupture propagating from Nucleation A. They will never turn into the seismic slip event, as shown in Figure 3b, due to the energy restoration of the fault system.

3.3 Accelerating Slow Slip Sequences Triggered by Early Seismic Events

To explore the interaction between preseismic slow slip events during nucleation and a fast slip event, we introduce a weakening perturbation zone (WPZ) to trigger a small seismic event during nucleation. In the WPZ, μ_{part} is set initially to 0.20, which is the same as the rest of the fault interface. At a certain time prior to the onset of the instability, we decrease μ_{part} within the WPZ to 0, simulating a small foreshock. Shortly after 100 sec (100 increments with 100 cycles/increment), μ_{part} in the WPZ is changed back to 0.20. Here, we define the time difference between the triggered seismic event and the reference event as the advanced time, and the corresponding occurrence of the time-advanced slip is the clock advance. In the following experiments, we vary the location and sizes of the WPZ at different times.

We first vary the location of a 5-km wide WPZ to create different scenarios, whereas the timing when we place the WPZ is the same for each case (2500.1 min). The time-space map of the slip rate for each case is plotted to show the triggering process (Figure 4). When the WPZ is placed at 10 km at 2500.1 min, which is close to Nucleation A (Case 1 in Figure 4a), the small earthquake initiates the large dynamic rupture instantaneously, an end-member of clock

advance, consistent with the process described by the cascade nucleation model. Moreover, the slip pattern and amplitude (Figure 4a) differ from those produced by the reference model (Figure 2c). However, as the WPZ is placed at 25 km or 45 km, both far away from any nucleation zone (Case 2 in Figures 4b and Case 4 in Figure 4d), only the small triggered earthquake takes place at 2500.1 min in each case, breaking the fault partially due to the dynamic weakening that we have imposed. Although Nucleation A at 12 km leads to a small clock advance, its slip pattern and magnitude are similar to those in the reference model (Figures 4b and 4d). Interestingly, Nucleation B and C are much smaller than Nucleation A, yet the small earthquake introduced at 35 km can still induce a large seismic event instantaneously, following the cascade nucleation mode (Case 3 in Figure 4c). Moreover, the slip pattern of the final seismic event in Case 3 differs from the reference case in Figure 2c.

Next, we also vary the width of the WPZ to explore how the distance between the foreshock and the preseismic slip events of Nucleation A, as well as the foreshock size affect the occurrence of cascade nucleation. The different advanced time durations (time differences between the triggered event and the reference event) produced are plotted in Figure 5a. As the distance between the preseismic slip events and the small earthquake increases, the advanced time decreases. Furthermore, as the size of the small earthquake increases, represented by the increase in WPZ width, the advanced time increases. Additionally, the possibility that the small earthquake instantaneously triggers a large seismic event, i.e., governed by cascade nucleation, decreases drastically as the foreshock occurrence is over 5 km away from the nucleation (white circles in Figure 5a). In addition, as the size of the foreshock is sufficiently small, the foreshock at the nucleation site does not instantaneously trigger a large seismic event. Instead, it causes a relatively large clock advance (orange circle at the bottom left corner in Figure 5a).

Finally, to showcase how the timing of the small earthquake influences the occurrence of cascade nucleation at Nucleation A, we also introduce the same width of the WPZ (5 km) at different times. In the early stage of the stick-slip cycle (~ 1200 min prior to reference failure in Figure 5b), the introduction of the WPZ always triggers a small clock advance of a seismic event, yet the timing of the small earthquake does not change the clock advance significantly. In contrast, if the foreshock occurs within ~ 1200 min prior to the reference seismic event, the advanced time increases dramatically (Figure 5b). As the system approaches the instability (after ~ 1200 min), the later the foreshock occurs, the larger the advanced time is, implying a higher possibility for the occurrence of cascade nucleation (Figure 5b). If the small foreshock occurs next to Nucleation A (blue curve in Figure 5b) ~ 200 min prior to the reference seismic event, the foreshock triggers the seismic event instantaneously. The relationship between the timing of the foreshock and the advanced time during the late stage of nucleation is nonlinearly inverse, in agreement with the discussion of the delayed triggering mechanism (Blank et al., 2021), which is caused by the acceleration of aseismic slip and stress change after ~ 1800 min in our numerical simulation (Figure 2c).

and Figure S1 in supplementary materials).

In summary, the foreshock caused by the introduction of WPZ can trigger a large cascade rupture nucleation as it is close to a nucleation zone that can potentially turn into a large dynamic rupture (Figures 4a and 4c). Furthermore, our simulation results show that the size and timing of the small earthquake, as well as the distance between the preseismic slow slip events of the nucleation site and the small earthquake, jointly determine whether the cascade nucleation can take place (Figure 5).

4 Discussion

4.1 Rupture Nucleation Process Reconciling Pre-slip and Cascade Models

Our reference model exhibits that multiple dynamic slip preparation sites may occur concurrently, governed by the pre-slip nucleation mode, and subjected to a heterogeneous stress state along the irregular geometric fault interface (Figure 2b). The accelerating preseismic slow slip sequences are a byproduct of a large nucleation process, consistent with previous observations of pre-slip rupture initiation processes (Cattania & Segall, 2021; McLaskey & Lockner, 2014; Yamashita et al., 2021).

In addition to the pre-slip nucleation mode processes, our model provides insights into interplays among different processes. The dynamic rupture produced from one nucleation site may propagate to neighboring segments, overprinting the growth of the aseismic slip events in other nucleation sites (Figures 2b and 2d). Moreover, if a sufficiently large foreshock occurs close enough to one cluster of precursory slow slip sequences, the foreshock may trigger a clock advance of the seismic event, substantially shortening the temporal earthquake initiation process (Figures 4 and 5).

To reconcile the pre-slip and cascade nucleation models, we propose rupture nucleation processes along a geometrically heterogeneous fault based on our numerical simulation results (Figures 6a and 6b). Multiple preseismic slow slip sequences represent different nucleation processes in the early stage of a rupture cycle (Figure 6a). As the variation in normal stress results from the fault's heterogeneity, a few preseismic slow slip sequences accelerate. The rest may be sparse aseismic slip events or slow earthquakes over the fault, which do not continue accelerating (Caniven et al., 2021). From geodetic and seismic records, we occasionally observe multiple aseismic slip events prior to the main shock. Each of them may be a candidate for precursory slow slip (black, red, blue, green, and brown nucleation sites in Figure 6a). A few of them may turn into small earthquakes (EQ 1 and EQ 2 in green and red, respectively, in Figure 6a), threatening to initiate nearby nucleation sites. If either EQ 1 or EQ 2 is sufficient to trigger a notable clock advance of the seismic event, the fault system will behave as the cascade nucleation model (Figure 6a). Therefore, a temporal and spatial gap appears between the expansion of the accelerating aseismic slip events and EQ 4 (blue nucleation site in Figure 6a), similar to the simulation results shown in Figures 4a and 4c. However, if EQ 1 and EQ

2 are not sufficiently large or close enough to trigger other nucleation sites instantaneously, as demonstrated by Figures 4b and 4d, the aseismic slip clusters in black will lead to the seismic event (EQ 3 in Figure 6b), generally following the pre-slip nucleation mode. However, there are likely a few preseismic slow slip events (clusters in blue and brown in Figure 6b) that may also have been experiencing acceleration and expansion prior to EQ 3, giving rise to difficulties in quantifying the growth of the slip patch and estimating the timing of EQ 3. Moreover, a large amount of elastic strain energy is released after EQ 3, resulting in a reset of the fault system. Hence, the blue and brown nucleation sites will never turn into other seismic events before entering the next seismic cycle (EQ 4 and EQ 5 in Figure 6b). An analog case is shown in Figure 3b, where Nucleation B and Nucleation C have the potential to lead up to a large seismic event but will never do due to the preceding energy release triggered by Nucleation A.

To conclude, the final seismic event is the result of contributions from multiple nucleation sites. Depending on the in-situ heterogeneity of the fault interface, the rupture process can ultimately appear to be comparable to either pre-slip, cascade up, or in between. Moreover, our simulation results reveal that pre-seismic slow slip sequences, experiencing acceleration and possessing features prone to turning into a dynamic slip event, are not necessarily the precursory slip processes (e.g., slow slip events in blue and brown nucleation sites, Figure 6b).

4.2 Characteristics of Non-precursory and Precursory Slow Slip and Their Implications for Seismic Hazard Assessment

4.2.1 Generation of Precursory Slow Slip

In our DEM models, fault roughness is created by a combination of the interlocked structure between identical size particles and a large-wavelength undulating topography resulting from a naturally emergent bend of the interface during the consolidation phase (Figure 1b). The geometric roughness controls the stress distributions (Figure 2b and Figure S1 in supplementary materials), resulting in variations in the apparent friction (τ/σ_n) along the fault. The location of the strongest geometric asperity usually implies a maximum apparent frictional strength, which correlates to the source of the seismic event (Caniven et al., 2017).

As the strongest geometric asperity starts to shear, the corresponding particles from the upper block climb up the ones of the lower block from the interlocked state (Figures S2a and S2b in supplementary materials). Overcoming the geometric asperity resistance, void spaces between the lower and upper blocks gradually dilate, reducing the area of contact areas along the sliding interface. Consequently, the fault dilation promotes a drop in frictional strength, leading to precursory slow slip sequences and their accelerations (Caniven et al., 2021). Once the asperity apex is reached (Figure S2c), resistance to the particle slip-page vanishes, enabling fast seismic slip, accompanied by a rapid shear-induced

closure of the void spaces (Figures S2d and S2e in supplementary materials), implying localized contraction states (Blank et al., 2021; Caniven et al., 2021). Eventually, the fault enters another interlocking state, indicating the end of one stick-slip cycle. The preseismic slow slip sequences that can evolve into fast seismic events are likely found at a highly dilatant sliding surface, potentially storing large elastic strain energy during the interseismic period (Caniven et al., 2021).

4.2.2 Two Types of Non-precursory Slow Slip, One of Which Can still be Dangerous

Not every preseismic slow slip sequence will lead up to a large dynamic slip event. One apparent feature possessed by the most typical non-precursory slow slip is its limited acceleration and maybe noticeable deceleration, controlled by a few additional factors, including thermal pressurization (Bizzarri & Cocco, 2006), shear-induced dilatancy (Dal Zilio et al., 2020; Segall et al., 2010), and fault topography (Caniven et al., 2021). In particular, Caniven et al. (2021) have inferred that a preseismic slow slip nucleation point, which restrains the fault dilation and the subsequent contraction, opposes the transition from aseismic slip events to a large dynamic.

In contrast, our simulation results reveal another type of non-precursory slow slip, which initiates from the fault roughness favoring dynamic rupture and causes acceleration in the aseismic phase prior to the seismic event (slow slip events in Nucleation B and Nucleation C in Figure 2c). Previous observations show multiple slow slip activities during a progressive increase in seismicities before the large megathrust earthquakes in the northeast Japan Arc and the south-central Chile Margin (Hasegawa & Yoshida, 2015; Socquet et al., 2017). Based on our simulation results, we suspect that many of these events may lead to different earthquakes, similar to the scenarios captured in Figures 6a and 6b. As a nearby seismic event occurs early, the stress state resets over the region, preventing the preseismic slow slip events from leading up to any dynamic rupture (Figures 6a and 6b). Therefore, they should not be defined as precursory slip processes for the incoming earthquake.

Interestingly, the accelerating preseismic slow slip events that are not directly related to the incoming pre-slip mode rupture nucleation, may be indicative of a local seismic hazard, and potentially triggered by small seismic events governed by the cascade nucleation mode (Figure 4c). It is reasonable to infer that the presence of regional accelerating aseismic slip events and aseismic bursts may imply that the corresponding region possesses the physical features, such as relatively strong relief asperities (as discussed in Section 4.2.1), that favor the production of large seismic events (e.g., Nucleation B and Nucleation C in Figure 2). The growth of those accelerating aseismic slip clusters may be slower than those in the neighboring segment. However, the region still maintains the potential to be triggered, producing a large seismic rupture (e.g., Nucleation B and Nucleation C in Figure 4c). This mechanism is manifested in Figure 6c and may help explain the unexpected occurrence of the 2020 Oct Mw 7.6 earth-

quake in the Shumagin Gap (Crowell & Melgar, 2020; Herman & Furlong, 2021). The 2020 Oct Mw 7.6 rupture zone appeared weakly coupled, compared to the adjacent 1946 and 1938 earthquake rupture segments. However, it is probable that the 2020 Jul Mw 7.8 earthquake took place nearby first, and its subsequent aftershock ruptured across the coupled region into a “pseudo-coupled” zone, triggering the 2020 Oct Mw 7.6 earthquake (Herman & Furlong, 2021). This scenario is comparable to our case shown in Figure 4c, where Nucleation B and Nucleation C initiate in the “pseudo-coupled” zone. The zone favors the generation of pre-slip nucleation mode rupture less than Nucleation A, yet still possesses a relatively high potential to be triggered seismically by a small seismic event (Figures 4c and 6c).

5 Conclusions

This study uses 2-D DEM models to simulate the rupture nucleation process, including slow (aseismic) and fast (dynamic) slip, on simplified, controlled, highly dilatant, and rough fault surfaces. Our models yield multiple nucleation sites prior to a seismic event, of which preseismic slow slip sequences were usually defined as precursory slip processes. In contrast to previous interpretations of precursory slow slip, the aseismic slip clusters in one nucleation site prove to be directly responsible for the incoming seismic events, while the preseismic slow slip events in the other nucleation sites may have a minimal effect on the impending seismic rupture.

Moreover, our simulation results demonstrate that the size and timing of the small earthquakes, as well as the distance between the preseismic slow slip events in the nucleation site and such small earthquakes, jointly control the clock advance of the seismic event and the occurrence of the cascade rupture nucleation. Furthermore, the simulation results suggest that the final seismic event likely results from multiple nucleation sites. We propose a mixed nucleation rupture process based on the numerical results, including two-end member nucleation models. Depending on the in-situ heterogeneity of the fault interface, the rupture process ultimately appears to be comparable to either a pre-slip, cascade-up, or in-between mode.

Lastly, our numerical simulations highlight the significance of characterizing preseismic accelerating aseismic slip sequences, which may indicate incoming seismic hazards. The numerical models yield two types of accelerating preseismic slow slip before the main event: 1) precursory slow slip clusters, which are accelerating and mainly governed by pre-slip nucleation mode, directly leading up to the next seismic event, and 2) accelerating preseismic slow slip events, which are a new type of non-precursory slow slip, representing the region favoring a seismic event, governed by pre-slip nucleation mode but non-correlated to the incoming main event. We infer that many accelerating preseismic slow slip sequences found prior to large historical earthquakes may be mislabeled as precursory slip processes. Moreover, these non-precursory accelerating aseismic slip events in nature could imply a potential seismic hazard that can be triggered by a dynamic rupture propagating from a neighboring segment.

Acknowledgments and Data

We thank Dr. Yanick Caniven (University of Oxford) for the helpful discussions. The data from all simulations of this research can be found in the published dataset on the ETH research collection: doi.org/10.3929/ethz-b-000577745.

Figures

Figure 1 (a) Schematics of two-end member nucleation models: pre-slip nucleation model (left) and cascade nucleation model (right). (b) DEM Model setup.

Figure 2 Simulation results of reference model without perturbation. (a) Plot of shear to normal stress ratio on servo walls and maximum slip rate at fault. (b) Plot of incremental change in shear stress near failure. The blue color represents a decrease in shear stress, and the red color represents an increase in shear stress. (c) Time-space map of slip rate near failure. (d) Plot of incremental change in mean stress demonstrates stress transfer through rupture initiation in reference model without perturbation. The blue color represents a decrease in the mean stress (local extension), and the red color represents an increase in the mean stress (local compression).

Figure 3 (a) Time-space map of slip rate after isolating Nucleation B and Nucleation C (refer to the reference model in Figure 2) by placing a 5-km-wide strengthening perturbation zone (SPZ) at 35 km in early phase of earthquake preparation. (b) Time-space map of slip rate after isolating Nucleation A (refer to the reference model in Figure 2) by placing a 10-km-wide SPZ at 10 km in early phase of earthquake preparation.

Figure 4 Time-space map of slip rate after a 5-km-wide weakening perturbation zone (WPZ) is placed to trigger a foreshock at 10 km (a), 20 km (b), 35 km (c), and 45 km (d) along a fault.

Figure 5 (a) Different sizes of small seismic events trigger clock advance from different distances to aseismic slip events in Nucleation A. The width of the weakening perturbation zone (WPZ) represents the size of the small seismic event. Different colors in circles represent the advanced time after the onset of the small seismic event, which is the time difference between the triggered seismic event and the reference event. A white circle represents the case where the seismic event is triggered instantaneously after the onset of the small seismic event. (b) A same-size small seismic event occurs at different timings from different distances to aseismic slip events in Nucleation A. Different colors represent the distance between the 5-km wide WPZ and the aseismic slip events in Nucleation A. The peak point in the blue curve indicates the instantaneously triggered seismic event (cascade rupture nucleation).

Figure 6 Schematic interpretation of earthquake initiation processes, reconciling two-end members of nucleation modes. The fault is presumably controlled by geometric topography only. Only the accelerating preseismic slow slip sequences are presented. (a) Earthquake preparation includes both nucleation modes but is mainly governed by cascade nucleation mode. (b) Earthquake preparation

includes both nucleation modes but is primarily governed by pre-slip nucleation mode. (c) Interpretation of an unexpected large seismic event in a “pseudo-couple” region triggered by a preceding seismic event across from a neighboring rupture zone.

References

- Albertini, G., Karrer, S., Grigoriu, M. D., and Kammer, D. S. (2021). Stochastic Properties of Static Friction. *Journal of the Mechanics and Physics of Solids*, **147**, 104242.
- Ampuero, J. P., and Rubin, A. M. (2008). Earthquake Nucleation on Rate and State Faults—Aging and Slip Laws. *Journal of Geophysical Research: Solid Earth*, **113**(B1).
- Barbot, S. (2019). Slow-Slip, Slow Earthquakes, Period-Two Cycles, Full and Partial Ruptures, and Deterministic Chaos in a Single Asperity Fault. *Tectonophysics*, **768**, 228171.
- Barker, D. H., Henrys, S., Caratori Tontini, F., Barnes, P. M., Bassett, D., Todd, E., and Wallace, L. (2018). Geophysical Constraints on the Relationship between Seamount Subduction, Slow Slip, and Tremor at the North Hikurangi Subduction Zone, New Zealand. *Geophysical Research Letters*, **45**(23), 12,804-812,813.
- Bilek, S. L., Schwartz, S. Y., and DeShon, H. R. (2003). Control of Seafloor Roughness on Earthquake Rupture Behavior. *Geology*, **31**(5), 455-458.
- Bizzarri, A., and Cocco, M. (2006). A Thermal Pressurization Model for the Spontaneous Dynamic Rupture Propagation on a Three-Dimensional Fault: 1. Methodological Approach. *Journal of Geophysical Research: Solid Earth*, **111**(B5).
- Blank, D., Morgan, J., and Caniven, Y. (2021). Geometrically Controlled Slow Slip Enhanced by Seismic Waves: A Mechanism for Delayed Triggering. *Earth and Planetary Science Letters*, **554**, 116695.
- Byerlee, J. (1978). Friction of Rocks. in *Rock Friction and Earthquake Prediction*. edited, pp. 615-626, Springer.
- Caniven, Y., Dominguez, S., Soliva, R., Peyret, M., Cattin, R., and Maerten, F. (2017). Relationships between Along-Fault Heterogeneous Normal Stress and Fault Slip Patterns During the Seismic Cycle: Insights from a Strike-Slip Fault Laboratory Model. *Earth and Planetary Science Letters*, **480**, 147-157.
- Caniven, Y., Morgan, J. K., and Blank, D. G. (2021). The Role of Along-Fault Dilatancy in Fault Slip Behavior. *Journal of Geophysical Research: Solid Earth*, e2021JB022310.
- Cattania, C., and Segall, P. (2021). Precursory Slow Slip and Foreshocks on Rough Faults. *Journal of Geophysical Research: Solid Earth*, **126**(4), e2020JB020430.
- Crowell, B. W., and Melgar, D. (2020). Slipping the Shumagin Gap: A Kinematic Coseismic and Early Afterslip Model of the Mw 7.8 Simeonof Island, Alaska, Earthquake. *Geophysical Research Letters*, **47**(19), e2020GL090308.
- Dal Zilio, L., Lapusta, N., and Avouac, J. P. (2020). Unraveling Scaling Properties of Slow-Slip Events. *Geophysical Research Letters*, **47**(10), e2020GL087477.
- Dalaison, M., Jolivet, R., van Rijnsingen, E., and Michel, S. (2021). The Interplay between Seismic and Aseismic Slip Along the Chaman Fault Illuminated by Insar. *Journal of Geophysical Research: Solid Earth*, **126**(12), e2021JB021935.
- Dieterich, J. (1978). Preseismic Fault Slip and Earthquake Prediction. *Journal of Geophysical Research: Solid Earth*, **83**(B8), 3940-3948.
- Dieterich, J. (1992). Earthquake

Nucleation on Faults with Rate-and State-Dependent Strength. *Tectonophysics*, **211**(1-4), 115-134. Dragert, H., Wang, K., and James, T. S. (2001). A Silent Slip Event on the Deeper Cascadia Subduction Interface. *Science*, **292**(5521), 1525-1528. Ellsworth, W., and Beroza, G. (1995). Seismic Evidence for an Earthquake Nucleation Phase. *Science*, **268**(5212), 851-855. Ferdowsi, B., and Rubin, A. M. (2020). A Granular Physics-Based View of Fault Friction Experiments. *Journal of Geophysical Research: Solid Earth*, **125**(6), e2019JB019016. Guérin-Marthe, S., Nielsen, S., Bird, R., Giani, S., and Di Toro, G. (2019). Earthquake Nucleation Size: Evidence of Loading Rate Dependence in Laboratory Faults. *Journal of Geophysical Research: Solid Earth*, **124**(1), 689-708. Hasegawa, A., and Yoshida, K. (2015). Preceding Seismic Activity and Slow Slip Events in the Source Area of the 2011 Mw 9.0 Tohoku-Oki Earthquake: A Review. *Geoscience Letters*, **2**(1), 1-13. Hawthorne, J., and Bartlow, N. (2018). Observing and Modeling the Spectrum of a Slow Slip Event. *Journal of Geophysical Research: Solid Earth*, **123**(5), 4243-4265. Herman, M. W., and Furlong, K. P. (2021). Triggering an Unexpected Earthquake in an Uncoupled Subduction Zone. *Science Advances*, **7**(13), eabf7590. Johnson, K. L. (1987). *Contact Mechanics*, Cambridge university press. Kato, A., and Ben-Zion, Y. (2021). The Generation of Large Earthquakes. *Nature Reviews Earth & Environment*, **2**(1), 26-39. Kato, A., Obara, K., Igarashi, T., Tsuruoka, H., Nakagawa, S., and Hirata, N. (2012). Propagation of Slow Slip Leading up to the 2011 Mw 9.0 Tohoku-Oki Earthquake. *Science*, **335**(6069), 705-708. Lapusta, N., and Rice, J. R. (2003). Nucleation and Early Seismic Propagation of Small and Large Events in a Crustal Earthquake Model. *Journal of Geophysical Research: Solid Earth*, **108**(B4). Leeman, J., Saffer, D., Scuderi, M., and Marone, C. (2016). Laboratory Observations of Slow Earthquakes and the Spectrum of Tectonic Fault Slip Modes. *Nature communications*, **7**(1), 1-6. McLaskey, G. C. (2019). Earthquake Initiation from Laboratory Observations and Implications for Foreshocks. *Journal of Geophysical Research: Solid Earth*, **124**(12), 12882-12904. McLaskey, G. C., and Lockner, D. A. (2014). Preslip and Cascade Processes Initiating Laboratory Stick Slip. *Journal of Geophysical Research: Solid Earth*, **119**(8), 6323-6336. Morgan, J. K. (2015). Effects of Cohesion on the Structural and Mechanical Evolution of Fold and Thrust Belts and Contractional Wedges: Discrete Element Simulations. *Journal of Geophysical Research: Solid Earth*, **120**(5), 3870-3896. Noda, H., Nakatani, M., and Hori, T. (2013). Large Nucleation before Large Earthquakes Is Sometimes Skipped Due to Cascade-up—Implications from a Rate and State Simulation of Faults with Hierarchical Asperities. *Journal of Geophysical Research: Solid Earth*, **118**(6), 2924-2952. Ohnaka, M., and Kuwahara, Y. (1990). Characteristic Features of Local Breakdown near a Crack-Tip in the Transition Zone from Nucleation to Unstable Rupture During Stick-Slip Shear Failure. *Tectonophysics*, **175**(1-3), 197-220. Olson, E. L., and Allen, R. M. (2005). The Deterministic Nature of Earthquake Rupture. *Nature*, **438**(7065), 212-215. Ozawa, S., Murakami, M., Kaidzu, M., Tada, T., Sagiya, T., Hatanaka, Y., Yarai, H., et al. (2002). Detection and Monitoring of Ongoing Aseismic Slip in the Tokai Region, Central Japan. *Science*, **298**(5595), 1009-1012. Peng, Z., and Gombert, J. (2010). An Integrated Perspective of the Continuum between

Earthquakes and Slow-Slip Phenomena. *Nature Geoscience*, **3**(9), 599-607.

Rice, J. R., Lapusta, N., and Ranjith, K. (2001). Rate and State Dependent Friction and the Stability of Sliding between Elastically Deformable Solids. *Journal of the Mechanics and Physics of Solids*, **49**(9), 1865-1898.

Romanet, P., Bhat, H. S., Jolivet, R., and Madariaga, R. (2018). Fast and Slow Slip Events Emerge Due to Fault Geometrical Complexity. *Geophysical Research Letters*, **45**(10), 4809-4819.

Ruiz, S., Metois, M., Fuenzalida, A., Ruiz, J., Leyton, F., Grandin, R., Vigny, C., et al. (2014). Intense Foreshocks and a Slow Slip Event Preceded the 2014 Iquique Mw 8.1 Earthquake. *Science*, **345**(6201), 1165-1169.

Sainoki, A., and Mitri, H. S. (2016). Instantaneous Stress Release in Fault Surface Asperities During Mining-Induced Fault-Slip. *Journal of Rock Mechanics and Geotechnical Engineering*, **8**(5), 619-628.

Segall, P., Rubin, A. M., Bradley, A. M., and Rice, J. R. (2010). Dilatant Strengthening as a Mechanism for Slow Slip Events. *Journal of Geophysical Research: Solid Earth*, **115**(B12).

Shäfer, J., Dippel, S., and Wolf, D. (1996). Force Schemes in Simulations of Granular Materials. *Journal de physique I*, **6**(1), 5-20.

Socquet, A., Valdes, J. P., Jara, J., Cotton, F., Walpersdorf, A., Cotte, N., Specht, S., et al. (2017). An 8 Month Slow Slip Event Triggers Progressive Nucleation of the 2014 Chile Megathrust. *Geophysical Research Letters*, **44**(9), 4046-4053.

Tape, C., Holtkamp, S., Silwal, V., Hawthorne, J., Kaneko, Y., Ampuero, J. P., Ji, C., et al. (2018). Earthquake Nucleation and Fault Slip Complexity in the Lower Crust of Central Alaska. *Nature Geoscience*, **11**(7), 536-541.

Trugman, D. T., and Ross, Z. E. (2019). Pervasive Foreshock Activity across Southern California. *Geophysical Research Letters*, **46**(15), 8772-8781.

Van den Ende, M., Chen, J., Ampuero, J.-P., and Niemeijer, A. (2018). A Comparison between Rate-and-State Friction and Microphysical Models, Based on Numerical Simulations of Fault Slip. *Tectonophysics*, **733**, 273-295.

Vora, H. B., and Morgan, J. K. (2019). Microscale Characterization of Fracture Growth and Associated Energy in Granite and Sandstone Analogs: Insights Using the Discrete Element Method. *Journal of Geophysical Research: Solid Earth*, **124**(8), 7993-8012.

Wang, X., Morgan, J. K., and Bangs, N. (2021). Relationships among Forearc Structure, Fault Slip, and Earthquake Magnitude: Numerical Simulations with Applications to the Central Chilean Margin. *Geophysical Research Letters*, **48**(13), e2021GL092521.

Yabe, S., and Ide, S. (2018). Variations in Precursory Slip Behavior Resulting from Frictional Heterogeneity. *Progress in Earth and Planetary Science*, **5**(1), 1-11.

Yamashita, F., Fukuyama, E., Xu, S., Kawakata, H., Mizoguchi, K., and Takizawa, S. (2021). Two End-Member Earthquake Preparations Illuminated by Foreshock Activity on a Meter-Scale Laboratory Fault. *Nature communications*, **12**(1), 1-11.